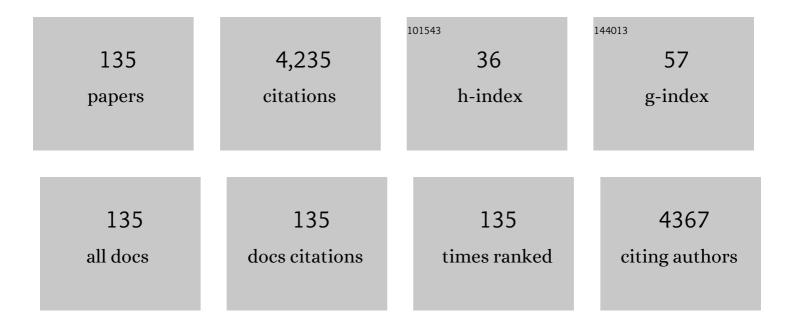
## Shuo Shi

List of Publications by Year in descending order

Source: https://exaly.com/author-pdf/7185092/publications.pdf Version: 2024-02-01



#	Article	IF	CITATIONS
1	Multichannel Interconnection Decomposition for Hyperspectral LiDAR Waveforms Detected From Over 500 m. IEEE Transactions on Geoscience and Remote Sensing, 2022, 60, 1-14.	6.3	9
2	Biodegradable oxygen-producing manganese-chelated metal organic frameworks for tumor-targeted synergistic chemo/photothermal/ photodynamic therapy. Acta Biomaterialia, 2022, 138, 463-477.	8.3	38
3	Nucleic Acid Architectonics for pH-Responsive DNA Systems and Devices. ACS Omega, 2022, 7, 3167-3176.	3.5	13
4	Tracking of Land Reclamation Activities Using Landsat Observations—An Example in Shanghai and Hangzhou Bay. Remote Sensing, 2022, 14, 464.	4.0	5
5	Target Classification of Similar Spatial Characteristics in Complex Urban Areas by Using Multispectral LiDAR. Remote Sensing, 2022, 14, 238.	4.0	28
6	A convolution neural network for forest leaf chlorophyll and carotenoid estimation using hyperspectral reflectance. International Journal of Applied Earth Observation and Geoinformation, 2022, 108, 102719.	2.8	11
7	Dual-Responsive and ROS-Augmented Nanoplatform for Chemo/Photodynamic/Chemodynamic Combination Therapy of Triple Negative Breast Cancer. ACS Applied Materials & Interfaces, 2022, 14, 57-68.	8.0	32
8	The Mechanisms of IncRNA-Mediated Multidrug Resistance and the Clinical Application Prospects of IncRNAs in Breast Cancer. Cancers, 2022, 14, 2101.	3.7	11
9	Leaf pigment retrieval using the PROSAIL model: Influence of uncertainty in prior canopy-structure information. Crop Journal, 2022, 10, 1251-1263.	5.2	11
10	Treatment of triple negative breast cancer by near infrared light triggered mild-temperature photothermal therapy combined with oxygen-independent cytotoxic free radicals. Acta Biomaterialia, 2022, 148, 218-229.	8.3	18
11	A Fe(III)-porphyrin-oxaliplatin(IV) nanoplatform for enhanced ferroptosis and combined therapy. Journal of Controlled Release, 2022, 348, 660-671.	9.9	32
12	Using HSI Color Space to Improve the Multispectral Lidar Classification Error Caused by Measurement Geometry. IEEE Transactions on Geoscience and Remote Sensing, 2021, 59, 3567-3579.	6.3	15
13	A novel STAT3 inhibitor W2014-S regresses human non-small cell lung cancer xenografts and sensitizes EGFR-TKI acquired resistance. Theranostics, 2021, 11, 824-840.	10.0	50
14	A PDA-DTC/Cu–MnO2 nanoplatform for MR imaging and multi-therapy for triple-negative breast cancer treatment. Chemical Communications, 2021, 57, 4158-4161.	4.1	14
15	An artificial intelligence process of immunoassay for multiple biomarkers based on logic gates. Analyst, The, 2021, 146, 889-895.	3.5	2
16	Application of Hyperspectral LiDAR on 3-D Chlorophyll-Nitrogen Mapping of Rohdea Japonica in Laboratory. IEEE Journal of Selected Topics in Applied Earth Observations and Remote Sensing, 2021, 14, 9667-9679.	4.9	10
17	Improving the Selection of Vegetation Index Characteristic Wavelengths by Using the PROSPECT Model for Leaf Water Content Estimation. Remote Sensing, 2021, 13, 821.	4.0	9
18	M2â€Like TAMs Function Reversal Contributes to Breast Cancer Eradication by Combination Dual Immune Checkpoint Blockade and Photothermal Therapy. Small, 2021, 17, e2007051.	10.0	34

#	Article	IF	CITATIONS
19	Analyzing the effect of incident angle on echo intensity acquired by hyperspectral lidar based on the Lambert-Beckman model. Optics Express, 2021, 29, 11055.	3.4	7
20	The Effect of Principal Component Analysis Parameters on Solar-Induced Chlorophyll Fluorescence Signal Extraction. Applied Sciences (Switzerland), 2021, 11, 4883.	2.5	0
21	Nanoparticleâ€Mediated siRNA Delivery and Multifunctional Modification Strategies for Effective Cancer Therapy. Advanced Materials Technologies, 2021, 6, 2001236.	5.8	13
22	Optical system design for a hyperspectral imaging lidar using supercontinuum laser and its preliminary performance. Optics Express, 2021, 29, 17542.	3.4	9
23	Exploiting a New Approach to Destroy the Barrier of Tumor Microenvironment: Nano-Architecture Delivery Systems. Molecules, 2021, 26, 2703.	3.8	12
24	True color 3D imaging optimization with missing spectral bands based on hyperspectral LiDAR. Optics Express, 2021, 29, 20406.	3.4	4
25	True-Color Reconstruction Based on Hyperspectral LiDAR Echo Energy. Remote Sensing, 2021, 13, 2854.	4.0	1
26	A self-amplified nanocatalytic system for achieving "1 + 1 + 1 > 3―chemody negative breast cancer. Journal of Nanobiotechnology, 2021, 19, 261.	namic ther	apy on triple
27	Optimized Estimation of Leaf Mass per Area with a 3D Matrix of Vegetation Indices. Remote Sensing, 2021, 13, 3761.	4.0	4
28	Improving characteristic band selection in leaf biochemical property estimation considering interrelations among biochemical parameters based on the PROSPECT-D model. Optics Express, 2021, 29, 400.	3.4	22
29	Metalâ€Polyphenolâ€Network Coated Prussian Blue Nanoparticles for Synergistic Ferroptosis and Apoptosis via Triggered GPX4 Inhibition and Concurrent In Situ Bleomycin Toxification. Small, 2021, 17, e2103919.	10.0	41
30	Land Cover Classification with Multispectral LiDAR Based on Multi-Scale Spatial and Spectral Feature Selection. Remote Sensing, 2021, 13, 4118.	4.0	16
31	Optimizing LUT-based inversion of leaf chlorophyll from hyperspectral lidar data: Role of cost functions and regulation strategies. International Journal of Applied Earth Observation and Geoinformation, 2021, 105, 102602.	2.8	4
32	Parameter Simulation and Design of an Airborne Hyperspectral Imaging LiDAR System. Remote Sensing, 2021, 13, 5123.	4.0	3
33	Post-synthesis strategy to integrate porphyrinic metal–organic frameworks with CuS NPs for synergistic enhanced photo-therapy. Journal of Materials Chemistry B, 2020, 8, 935-944.	5.8	29
34	A Ru <sup>II</sup> Polypyridyl Alkyne Complex Based Metal–Organic Frameworks for Combined Photodynamic/Photothermal/Chemotherapy. Chemistry - A European Journal, 2020, 26, 1668-1675.	3.3	29
35	Distributed Congestion Control via Outage Probability Model for Delay-Constrained Flying Ad Hoc Networks. Wireless Communications and Mobile Computing, 2020, 2020, 1-9.	1.2	2
36	A multifunctional SN38-conjugated nanosystem for defeating myelosuppression and diarrhea induced by irinotecan in esophageal cancer. Nanoscale, 2020, 12, 21234-21247.	5.6	13

#	Article	IF	CITATIONS
37	New Strategy for Reducing Tau Aggregation Cytologically by A Hairpinlike Molecular Inhibitor, Tannic Acid Encapsulated in Liposome. ACS Chemical Neuroscience, 2020, 11, 3623-3634.	3.5	14
38	Glucose Oxidaseâ€Related Cancer Therapies. Advanced Therapeutics, 2020, 3, 2000110.	3.2	42
39	Cytokine-induced killer cells-assisted tumor-targeting delivery of Her-2 monoclonal antibody-conjugated gold nanostars with NIR photosensitizer for enhanced therapy of cancer. Journal of Materials Chemistry B, 2020, 8, 8368-8382.	5.8	29
40	Hepatoprotective Angelica sinensis silver nanoformulation against multidrug resistant bacteria and the integration of a multicomponent logic gate system. Nanoscale, 2020, 12, 19149-19158.	5.6	2
41	Estimation of Multi-Species Leaf Area Index Based on Chinese GF-1 Satellite Data Using Look-Up Table and Gaussian Process Regression Methods. Sensors, 2020, 20, 2460.	3.8	18
42	Estimating leaf nitrogen concentration based on the combination with fluorescence spectrum and first-derivative. Royal Society Open Science, 2020, 7, 191941.	2.4	6
43	[Ru(phen) <sub>2</sub> podppz] <sup>2+</sup> significantly inhibits glioblastoma growth <i>in vitro</i> and <i>vivo</i> with fewer side-effects than cisplatin. Dalton Transactions, 2020, 49, 8864-8871.	3.3	8
44	Orientation-Inspired Perspective on Molecular Inhibitor of Tau Aggregation by Curcumin Conjugated with Ruthenium(II) Complex Scaffold. Journal of Physical Chemistry B, 2020, 124, 2343-2353.	2.6	15
45	Nanotechnologies for enhancing cancer immunotherapy. Nano Research, 2020, 13, 2595-2616.	10.4	22
46	A Cu9S5 nanoparticle-based CpG delivery system for synergistic photothermal-, photodynamic- and immunotherapy. Communications Biology, 2020, 3, 343.	4.4	29
47	Active 3D Imaging of Vegetation Based on Multi-Wavelength Fluorescence LiDAR. Sensors, 2020, 20, 935.	3.8	13
48	Leaf Biochemistry Parameters Estimation of Vegetation Using the Appropriate Inversion Strategy. Frontiers in Plant Science, 2020, 11, 533.	3.6	4
49	Assessing different regression algorithms for paddy rice leaf nitrogen concentration estimations from the first-derivative fluorescence spectrum. Optics Express, 2020, 28, 18728.	3.4	11
50	True-Color Three-Dimensional Imaging and Target Classification Based on Hyperspectral LiDAR. Remote Sensing, 2019, 11, 1541.	4.0	15
51	Potential of Fluorescence Index Derived from the Slope Characteristics of Laser-Induced Chlorophyll Fluorescence Spectrum for Rice Leaf Nitrogen Concentration Estimation. Applied Sciences (Switzerland), 2019, 9, 916.	2.5	6
52	Tumorâ€Targeted Drug and CpG Delivery System for Phototherapy and Docetaxelâ€Enhanced Immunotherapy with Polarization toward M1â€Type Macrophages on Triple Negative Breast Cancers. Advanced Materials, 2019, 31, e1904997.	21.0	238
53	A redox-activated theranostic nanoplatform: toward glutathione-response imaging guided enhanced-photodynamic therapy. Inorganic Chemistry Frontiers, 2019, 6, 2865-2872.	6.0	9
54	A new waveform decomposition method for multispectral LiDAR. ISPRS Journal of Photogrammetry and Remote Sensing, 2019, 149, 40-49.	11.1	32

#	Article	IF	CITATIONS
55	Luminescent Ru( <scp>ii</scp> )-thiol modified silver nanoparticles for lysosome targeted theranostics. Dalton Transactions, 2019, 48, 10393-10397.	3.3	15
56	G-quadruplex and duplex DNA binding studies of novel Ruthenium(II) complexes containing ascididemin ligands. Journal of Inorganic Biochemistry, 2019, 196, 110681.	3.5	17
57	Integrating <i>in situ</i> formation of nanozymes with mesoporous polydopamine for combined chemo, photothermal and hypoxia-overcoming photodynamic therapy. Chemical Communications, 2019, 55, 14785-14788.	4.1	44
58	Wavelength selection of the multispectral lidar system for estimating leaf chlorophyll and water contents through the PROSPECT model. Agricultural and Forest Meteorology, 2019, 266-267, 43-52.	4.8	48
59	Labelâ€free molecular probe based on Gâ€quadruplex and strand displacement for sensitive and selective detection and naked eye discrimination of exon 2 deletion of AIMP2. Chemical Biology and Drug Design, 2019, 93, 993-998.	3.2	3
60	Hyperspectral lidar point cloud segmentation based on geometric and spectral information. Optics Express, 2019, 27, 24043.	3.4	31
61	Effect of different regression algorithms on the estimating leaf parameters based on selected characteristic wavelengths by using the PROSPECT model. Applied Optics, 2019, 58, 9904.	1.8	2
62	Estimating leaf chlorophyll status using hyperspectral lidar measurements by PROSPECT model inversion. Remote Sensing of Environment, 2018, 212, 1-7.	11.0	36
63	Regulation of multi-factors (tail/loop/link/ions) for G-quadruplex enantioselectivity of Δ- and ĥ- [Ru(bpy)2(dppz-idzo)]2+. Dalton Transactions, 2018, 47, 5422-5430.	3.3	8
64	Analyzing the performance of PROSPECT model inversion based on different spectral information for leaf biochemical properties retrieval. ISPRS Journal of Photogrammetry and Remote Sensing, 2018, 135, 74-83.	11.1	43
65	Analyzing the Effect of Fluorescence Characteristics on Leaf Nitrogen Concentration Estimation. Remote Sensing, 2018, 10, 1402.	4.0	11
66	Potential of vegetation indices combined with laser-induced fluorescence parameters for monitoring leaf nitrogen content in paddy rice. PLoS ONE, 2018, 13, e0191068.	2.5	17
67	The application of time decay characteristics of laserâ€induced fluorescence in the classification of vegetation. Luminescence, 2017, 32, 17-21.	2.9	0
68	Quantitative Fluorescence Quenching on Antibody-conjugated Graphene Oxide as a Platform for Protein Sensing. Scientific Reports, 2017, 7, 40772.	3.3	32
69	Evaluation of hyperspectral LiDAR for monitoring rice leaf nitrogen by comparison with multispectral LiDAR and passive spectrometer. Scientific Reports, 2017, 7, 40362.	3.3	36
70	Monitoring of Paddy Rice Varieties Based on the Combination of the Laser-Induced Fluorescence and Multivariate Analysis. Food Analytical Methods, 2017, 10, 2398-2403.	2.6	9
71	Coordination polymer nanoparticles from nucleotide and lanthanide ions as a versatile platform for color-tunable luminescence and integrating Boolean logic operations. Nanoscale, 2017, 9, 9589-9597.	5.6	41
72	Integration of G-quadruplex and DNA-templated Ag NCs for nonarithmetic information processing. Chemical Science, 2017, 8, 4211-4222.	7.4	49

#	Article	IF	CITATIONS
73	The characterization of plant species using firstâ€derivative fluorescence spectra. Luminescence, 2017, 32, 348-352.	2.9	1
74	Combined application of 3D spectral features from multispectral LiDAR for classification. , 2017, , .		5
75	Effect of fluorescence characteristics and different algorithms on the estimation of leaf nitrogen content based on laser-induced fluorescence lidar in paddy rice. Optics Express, 2017, 25, 3743.	3.4	27
76	Multispectral LiDAR Point Cloud Classification: A Two-Step Approach. Remote Sensing, 2017, 9, 373.	4.0	43
77	Estimating Rice Leaf Nitrogen Concentration: Influence of Regression Algorithms Based on Passive and Active Leaf Reflectance. Remote Sensing, 2017, 9, 951.	4.0	49
78	Using Different Regression Methods to Estimate Leaf Nitrogen Content in Rice by Fusing Hyperspectral LiDAR Data and Laser-Induced Chlorophyll Fluorescence Data. Remote Sensing, 2016, 8, 526.	4.0	30
79	Analyzing the performance of fluorescence parameters in the monitoring of leaf nitrogen content of paddy rice. Scientific Reports, 2016, 6, 28787.	3.3	23
80	[Ru(L) 2 (3-tppp)] 2+ (L = bpy, phen) stabilizes two different forms of the human telomeric G-quadruplex DNA. Inorganic Chemistry Communication, 2016, 72, 7-12.	3.9	9
81	Excitation Wavelength Analysis of Laser-Induced Fluorescence LiDAR for Identifying Plant Species. IEEE Geoscience and Remote Sensing Letters, 2016, 13, 977-981.	3.1	14
82	Three label-free thrombin aptasensors based on aptamers and [Ru(bpy) <sub>2</sub> (o-mopip)] <sup>2+</sup> . Journal of Materials Chemistry B, 2016, 4, 1361-1367.	5.8	26
83	Laser-induced fluorescence characteristics of vegetation by a new excitation wavelength. Spectroscopy Letters, 2016, 49, 263-267.	1.0	19
84	Ultrasensitive and universal fluorescent aptasensor for the detection of biomolecules (ATP,) Tj ETQq0 0 0 rgBT /C Bioelectronics, 2016, 79, 205-212.	verlock 10 10.1	0 Tf 50 307 1 100
85	A universal label-free fluorescent aptasensor based on Ru complex and quantum dots for adenosine, dopamine and 17β-estradiol detection. Biosensors and Bioelectronics, 2016, 79, 198-204.	10.1	100
86	A RET-supported logic gate combinatorial library to enable modeling and implementation of intelligent logic functions. Chemical Science, 2016, 7, 1853-1861.	7.4	68
87	Estimation of rice leaf nitrogen contents based on hyperspectral LIDAR. International Journal of Applied Earth Observation and Geoinformation, 2016, 44, 136-143.	2.8	84
88	Binding Behaviors for Different Types of DNA Gâ€Quadruplexes: Enantiomers of [Ru(bpy) <sub>2</sub> (L)] <sup>2+</sup> (L=dppz, dppzâ€idzo). Chemistry - A European Journal, 2015, 21, 11435-11445.	3.3	40
89	Effect of the Ancillary Ligands on the Spectral Properties and Gâ€Quadruplexes DNA Binding Behavior: A Combined Experimental and Theoretical Study. Chemistry - A European Journal, 2015, 21, 13390-13400.	3.3	17
90	Investigating the Potential of Using the Spatial and Spectral Information of Multispectral LiDAR for Object Classification. Sensors, 2015, 15, 21989-22002.	3.8	41

#	Article	IF	CITATIONS
91	Improving Backscatter Intensity Calibration for Multispectral LiDAR. IEEE Geoscience and Remote Sensing Letters, 2015, 12, 1421-1425.	3.1	33
92	Vegetation identification based on characteristics of fluorescence spectral spatial distribution. RSC Advances, 2015, 5, 56932-56935.	3.6	10
93	Sensitive detection for coralyne and mercury ions based on homo-A/T DNA by exonuclease signal amplification. Biosensors and Bioelectronics, 2015, 71, 439-444.	10.1	19
94	Molecular "light switch―[Ru(phen) <sub>2</sub> dppzidzo] <sup>2+</sup> monitoring the aggregation of tau. Analyst, The, 2015, 140, 7513-7517.	3.5	11
95	Impacts of terminal modification of [Ru(phen) <sub>2</sub> dppz] <sup>2+</sup> on the luminescence properties: a theoretical study. Dalton Transactions, 2015, 44, 19264-19274.	3.3	13
96	Cu2+ modulated silver nanoclusters as an on–off–on fluorescence probe for the selective detection of l-histidine. Biosensors and Bioelectronics, 2015, 66, 103-108.	10.1	62
97	Ultrasensitive fluorescence detection of heparin based on quantum dots and a functional ruthenium polypyridyl complex. Biosensors and Bioelectronics, 2014, 55, 174-179.	10.1	43
98	Two structurally analogous ruthenium complexes as naked-eye and reversible molecular "light switch―for G-quadruplex DNA. Journal of Inorganic Biochemistry, 2014, 140, 64-71.	3.5	31
99	A label-free fluorescent probe for Hg2+ and biothiols based on graphene oxide and Ru-complex. Scientific Reports, 2014, 4, 5320.	3.3	45
100	[Ru(bpy)2dppz-idzo]2+: a colorimetric molecular "light switch―and powerful stabilizer for G-quadruplex DNA. Dalton Transactions, 2013, 42, 5661.	3.3	59
101	Label-free fluorescent DNA biosensors based on metallointercalators and nanomaterials. Methods, 2013, 64, 305-314.	3.8	19
102	A comparative study of the interaction of two structurally analogous ruthenium complexes with human telomeric G-quadruplex DNA. Journal of Inorganic Biochemistry, 2013, 121, 19-27.	3.5	34
103	A new fluorescence "switch on―assay for heparin detection by using a functional ruthenium polypyridyl complex. Analyst, The, 2013, 138, 3483.	3.5	25
104	Molecular Hairpin: A Possible Model for Inhibition of Tau Aggregation by Tannic Acid. Biochemistry, 2013, 52, 1893-1902.	2.5	41
105	Targeting Human Telomeric G-Quadruplex DNA and Inhibition of Telomerase Activity With [(dmb)2Ru(obip)Ru(dmb)2]4+. PLoS ONE, 2013, 8, e84419.	2.5	14
106	Label-free fluorescent DNA sensor for the detection of silver ions based on molecular light switch Ru complex and unmodified quantum dots. Analyst, The, 2013, 138, 421-424.	3.5	29
107	A Naked-Eye On–Off–On Molecular "Light Switch―Based on a Reversible "Conformational Switch― G-Quadruplex DNA. Inorganic Chemistry, 2012, 51, 12591-12593.	of 4.0	65
108	[Ru(bpy)2(bppp)]2+ binds two different forms of the human telomeric G-quadruplex structure. Inorganic Chemistry Communication, 2012, 24, 212-215.	3.9	12

#	Article	IF	CITATIONS
109	A molecular light switch Ru complex and quantum dots for the label-free, aptamer-based detection of thrombin. Analyst, The, 2012, 137, 1550.	3.5	22
110	Molecular "light switch―for G-quadruplex DNA: cycling the switch on and off. Dalton Transactions, 2012, 41, 5789.	3.3	40
111	Polypyridyl Complexes of Ruthenium(II): Stabilization of Gâ€quadruplex DNA and Inhibition of Telomerase Activity. ChemPlusChem, 2012, 77, 551-562.	2.8	18
112	Cooperative folding of tau peptide by coordination of group IIB metal cations during heparin-induced aggregation. BioMetals, 2012, 25, 361-372.	4.1	12
113	Graphene oxide–Ru complex for label-free assay of DNA sequence and potassium ions via fluorescence resonance energy transfer. Analytical Methods, 2011, 3, 2472.	2.7	39
114	The Impacts of Hg(II) Tightly Binding on the Alzheimer's Tau Construct R3: Misfolding and Aggregation. Bulletin of the Chemical Society of Japan, 2011, 84, 1362-1367.	3.2	5
115	Aqua[4′-(4-chlorophenyl)-2,2′:6′,2′′-terpyridine]nitratocopper(II) nitrate [4′-(4-chlorophenyl)-2,2′:6′,2′′-terpyridine]dinitratocopper(II) monohydrate. Acta Crystallographica Section E: Structure Reports Online, 2011, 67, m346-m346.	0.2	1
116	Flavonoids Inhibit Heparin-Induced Aggregation of the Third Repeat (R3) of Microtubule-Binding Domain of Alzheimer's Tau Protein. Bulletin of the Chemical Society of Japan, 2010, 83, 911-922.	3.2	6
117	Mercury(II) promotes the in vitro aggregation of tau fragment corresponding to the second repeat of microtubuleâ€binding domain: Coordination and conformational transition. Biopolymers, 2010, 93, 1100-1107.	2.4	18
118	Molecular "light switch―for G-quadruplexes and i-motif of human telomeric DNA: [Ru(phen)2(dppz)]2+. Dalton Transactions, 2010, 39, 2490.	3.3	84
119	Interaction of [Ru(bpy)2(dppz)]2+ with human telomeric DNA: Preferential binding to G-quadruplexes over i-motif. Biochimie, 2010, 92, 370-377.	2.6	108
120	Synthesis, characterization, and DNAâ€binding of chiral complexes Δ―and Λâ€{Ru(bpy) <sub>2</sub> (pyip)] <sup>2+</sup> . Chirality, 2009, 21, 276-283.	2.6	20
191	Synthesis, characterization, DNA-binding and DNA-photocleavage studies of [Ru(bpy)2(pmip)]2+ and		

#	Article	IF	CITATIONS
127	DFT/TDDFT studies on electronic absorption and emission spectra of [Ru(bpy)2(L)]2+ (L=pip, o-mopip and) Tj ETÇ	)q1_1 0.78 1.5	4314 rgBT
128	Experimental and theoretical studies on the DNA-binding and spectral properties of water-soluble complex [Ru(MeIm)4(dpq)]2+. Journal of Molecular Structure, 2008, 881, 156-166.	3.6	68
129	A combined computational and experimental study on DNA-photocleavage of Ru(ii) polypyridyl complexes [Ru(bpy)2(L)]2+ (L = pip, o-mopip and p-mopip). Dalton Transactions, 2008, , 291-301.	3.3	33
130	Promoting the Formation and Stabilization of G-Quadruplex by Dinuclear Rull Complex Ru2(obip)L4. Inorganic Chemistry, 2008, 47, 2910-2912.	4.0	79
131	1,2-Bis[amino(pyrimidin-2-yl)methylene]hydrazine dihydrate. Acta Crystallographica Section E: Structure Reports Online, 2008, 64, o272-o272.	0.2	3
132	Synthesis, characterization and DNA-binding of novel chiral complexes Δ- and ĥ-[Ru(bpy)2L]2+ (L=o-mopip) Tj ETG	Qg0_0 0 rg	BT /Overloci 146
133	Investigation on DNA Binding and Photo-Cleavage Properties of Water-Soluble Porphyrin and Metalloporphyrins. Transition Metal Chemistry, 2005, 30, 684-690.	1.4	6

134	Electronic effect of different positions of the –NO2 group on the DNA-intercalator of chiral complexes [Ru(bpy)2L]2+(L =0-npip, m-npip and p-npip). Dalton Transactions, 2005, , 2038.	3.3	84
135	Synthesis, characterization and antiviral activity against influenza virus of a series of novel manganese-substituted rare earth borotungstates heteropolyoxometalates. Antiviral Research, 2004, 62, 65-71.	4.1	46